Long Baseline Neutrino Oscillation Experiments

H. Gallagher
Tufts University, Medford, MA 02155, USA

In this paper I will review briefly the experimental results which established the existence of neutrino mixing, the current generation of long baseline accelerator experiments, and the prospects for the future. In particular I will focus on the recent analysis of the MINOS experiment.

1. Introduction

The experimental discovery of neutrino mixing and oscillations ranks as one of the most exciting discoveries of the past several decades. The phenomenon has now been observed in solar, atmospheric, reactor, and accelerator neutrino fluxes. The field is rapidly moving into a new generation of precision measurements which are requiring ever larger detectors and more powerful beams. In this section I will briefly summarize the discoveries of the past decade that have set us out on this exciting road.

1.1. Neutrino Masses and Mixing

The question of whether or not neutrinos have mass, and if so, exactly what form the neutrino masses take (Dirac or Majorana) has been a topic of speculation for some time. The relationship between the weak states and the mass states is given by a 3×3 unitary matrix called the Pontecorvo-Maki-Nakagawa-Sakata (PMNS) matrix after the founding role they played in the description of neutrino oscillations Maki et al. [1962], Pontecorvo [1968].

If neutrinos have mass then a neutrino created in an initial flavor eigenstate α evolves over time as a superposition of mass states with different phases. If detected some time later there is a non-zero probability that it can be detected as a different flavor. In a simplified two-generation case, which is often a good approximation when the probability is dominated by a single mass scale, the oscillation probability is:

$$P(\nu_\alpha \rightarrow \nu_\beta) = \sin^2(2\theta)\sin^2(1.27\Delta m^2 L/E) \qquad (1)$$

where θ is the mixing angle relating the weak and mass eigenstates, $\Delta m^2 = |m_1^2 - m_2^2|$ (eV^2), L is the distance the neutrinos have traveled (km), and E is the energy (GeV).

In a general three-flavor case there are 9 numbers we are interested in. Three neutrino masses (m_1, m_2, m_3), three mixing angles $(\theta_{12}, \theta_{23}, \theta_{13})$, and three CP-violating phases (δ_{CP},α_1, α_2). The latter two CP-violating phases are relevant only for Majorana neutrinos and play no role in oscillation phenomena. Experimental evidence for neutrino flavor change and oscillations currently come from five sources: solar neutrinos, atmospheric neutrinos, reactor neutrinos, accelerator neutrinos, and for neutrinos from μ^+ decay (LSND). It is not possible to accommodate all of these results in terms of three neutrino masses. The miniBoone experiment, currently running at Fermilab, is exploring the LSND result and will be able to resolve this important question.

Global fits to data from solar, atmospheric, reactor, and accelerator experiments Fogli et al. [2006a,b] indicate that the parameters associated with the oscillation of reactor and solar neutrinos are ($\delta m^2 = 7.92(1 \pm 0.09) \times 10^{-5}$eV^2, $\sin^2(\theta_{12}) = 0.314(1^{+0.18}_{-0.15})$), the atmospheric parameters are ($\Delta m^2 = 2.6(1^{+0.14}_{-0.15}) \times 10^{-3}$ eV^2, $\sin^2(\theta_{23}) = 0.45(1^{+0.35}_{-0.20})$), and $\sin^2(\theta_{13}) < 0.8^{+2.3}_{-0.8} \times 10^{-2}$. Uncertainties quoted here are 2σ values Fogli et al. [2006a,b].

The experimental understanding of the PMNS matrix prior to the results from the MINOS experiment is thoroughly summarized by B. Kayser in Reference Eidelman et al. [2004]. Setting aside LSND the neutrino mass and mixing matrix is summarized by Figure 1 Eidelman et al. [2004]. An additional open question is whether the mass hierarchy is 'Normal', as indicated by this Figure, or is 'Inverted', in which case the masses separated by the small mass splitting δm^2 lie above the 3rd mass state, and are separated from it by the large mass splitting Δm^2.

As these results indicate the parameters associated with the oscillation of atmospheric, reactor, solar, and atmospheric neutrinos are becoming increasingly well known, with precision on the order of 10-20%. The remaining mixing parameter θ_{13} is relatively poorly constrained, and nothing is known about the CP violating phase of the PMNS matrix. The main experimental goals for this field can therefore be broken down according to timescales:

1. **Questions for the current generation: miniBoone, MINOS, OPERA**
   (a) Is there mixing to a sterile 4th generation of neutrino (needed to accommodate LSND)?
   (b) Obtaining better precision on the dominant mixing parameters, i.e. is θ_{23} really45°?
   (c) Are we *really* seeing oscillations?

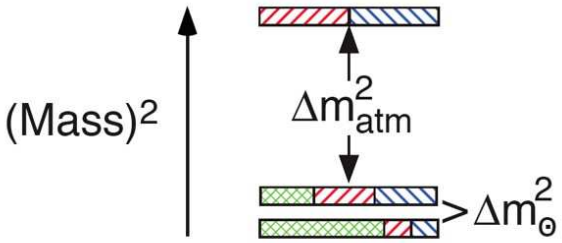

Figure 1: The 'normal hierarchy' of neutrino masses in a 3-generation framework which describes current experimental results with the exception of LSND. The ν_e component of each mass state is crosshatched, the ν_μ component is indicated by right-leaning hatching, and the ν_τ component is indicated by left-leaning hatching. From Reference Eidelman et al. [2004].

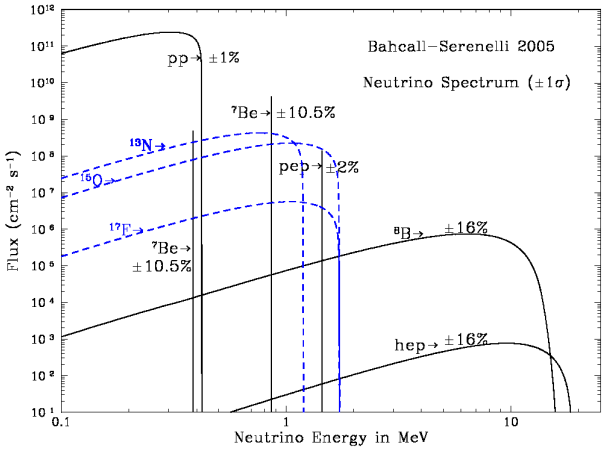

Figure 2: Solar neutrino energy spectra. Figure from Reference Bahcall et al. [2005].

(d) Can we confirm neutrino appearance $\nu_\mu \rightarrow \nu_\tau$?

2. **Questions for the Next Generation (T2K, NOνA)**

   (a) 'Normal' or 'Inverted' mass hierarchy.

   (b) Measuring θ_{13}.

   (c) Measuring δ_{CP}.

3. **Questions for Others (cosmology, neutrinoless beta decay, kinematic mass measurements)**

   (a) Are neutrinos degenerate? Can we determine m_ν rather than Δm^2?

   (b) Are neutrinos Dirac or Majorana particles?

1.2. Solar Neutrinos

Solar neutrinos have been a topic of intense experimental study for nearly 40 years. These neutrinos are produced by a variety of mechanisms in the sun and can be detected using several different techniques. The energy spectra of solar neutrinos from the 'Standard Solar Model' of Reference Bahcall et al. [2005] is shown in Figure 2.

The first experiments by Ray Davis and collaborators in the Homestake mine in South Dakota used the reaction $\nu_e + {}^{37}Cl \rightarrow {}^{37}Ar + e^-$ and counting of individual atoms of ^{37}Ar to measure the solar neutrino flux Cleveland et al. [1998]. These experiments were sensitive primarily to ^{8}B neutrinos from the sun. This experimental technique was refined over many years and consistently produced results which were in substantial disagreement with the solar model predictions of the time. The final result from the experiment is only about 1/3 of the expected value Cleveland et al. [1998]. Subsequent radiochemical experiments which used the conversion of gallium into germanium with lower energy thresholds and yielded results around 55% of the solar model Altmann et al. [2005], Hampel et al. [1999], Abdurashitov et al. [2002]. Real-time detection of neutrinos from neutrino-electron elastic scattering similarly showed substantial deficits Fukuda et al. [1996], Hosaka et al. [2006]. These results together were described as the 'solar neutrino puzzle'. The fact that the different experimental techniques measured different deficits compared with the prediction indicated that energy dependent - suppression mechanisms were at work.

Over the last five years data from the SNO and KamLAND experiments have definitively resolved the 'solar neutrino puzzle'. The SNO experiment in Ontario, Canada consists of 1 kton of ultra-pure heavy water in a 12-m diameter acrylic vessel surrounded by 9600 PMTs. SNO detects ^{8}B neutrinos through both the neutral current (NC) and charged current (CC) interactions as well as through elastic scattering from electrons (ES). The NC channel, a unique measurement capability to SNO, is particularly important as it measures the sum of all three active neutrino flavors. Figure 3 shows the results of the experiment as presented in Aharmim et al. [2005]. The measurements are consistent with the total flux predicted by the Standard Solar Model, but indicate that a majority of the flux has oscillated into muon and tau flavors which interact in the detector via NC channels but not CC channels. The explanation that emerged was one of electron neutrinos undergoing transitions to other flavors via a matter-enhancement of the mixing probability known as the Mikheyev-Smirnov-Wolfenstein (MSW) effect.

The interpretation of this data in terms of neutrino mixing was dramatically confirmed by the KamLAND experiment in 2002 Eguchi et al. [2003]. This exper-

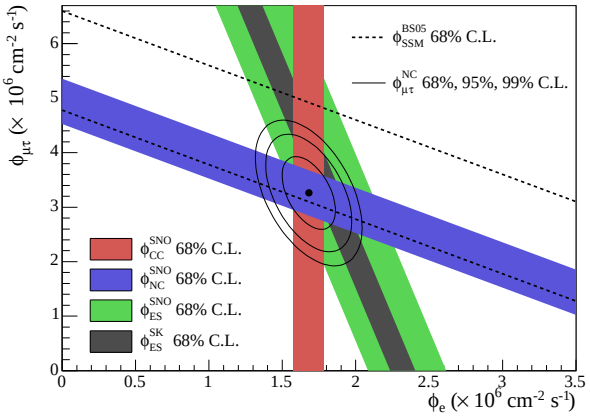

Figure 3: The flux of muon and tau neutrinos versus the flux of electron neutrinos as measured by the SNO experiment. Charged current (CC), neutral (NC) and elastic scattering (ES) results are given as bands. Dashed lines indicate the predictions for the total neutrino flux from Reference Bahcall et al. [2005]. Ovals indicate the 68, 95, and 99% CL intervals from the combined data Aharmim et al. [2005].

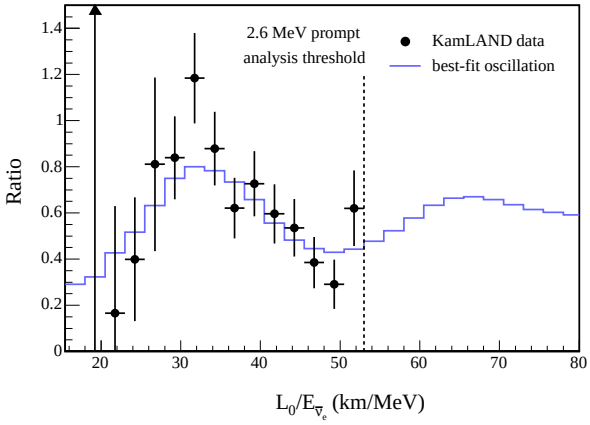

Figure 4: Ratio of the observed L/E spectrum from the KamLAND experiment to the no oscillation expectation. In this plot L is taken to be 180 km. The curve is the best fit oscillation result. Plot is from Araki et al. [2005].

iment utilized a 1-kton liquid scintillator detector located at the old Kamiokande site in Japan to make a long-baseline measurement of $\overline{\nu}_e$ from nuclear reactors. Because of the long baseline (hundreds of km) and neutrino energies (few MeV), this experiment is sensitive to the same oscillation parameter space explored by the solar experiments. The experiment observed 258 neutrino events where 365.2 ± 23.7 (syst.) were expected in the absence of oscillations Araki et al. [2005]. Figure 4 from Reference Araki et al. [2005] shows the L/E distribution for neutrinos measured by the KamLAND experiment, which also shows evidence for the spectral distortion expected from neutrino oscillations.

1.3. Atmospheric Neutrinos

Strong evidence for oscillation of neutrinos at the larger mass difference came from studies of atmospheric neutrinos. These measurements were initially being made as a way of understanding the dominant background for large nucleon decay experiments located in deep mines worldwide. These experiments failed to confirm even the most robust predictions of atmospheric flux models, the atmospheric neutrino flavor ratio. Since both electron flavor and muon flavor neutrinos are produced in the decay chain of pions, they should be present in a 1:2 ratio. High-statistics data from the Super-Kamiokande data, and confirmatory measurements by other, smaller experiments provided clear evidence of oscillations in the atmospheric neutrino flux with the dominant effect being the disappearance of muon neutrinos.

In many ways our first round of discoveries in the field of neutrino oscillations have been marked by good fortune. For neutrinos with Δm^2 around 10^{-3} eV^2, the earth is a perfect size for a neutrino oscillation experiment. Broadly speaking the atmospheric neutrino flux can be seen as two beams - one from neutrinos coming from above the horizon, which have not oscillated, and one from below the horizon, which have oscillated fully. Up vs. down and shape comparisons allow sensitive measurements of the oscillation parameters which cancel many of the uncertainties in the atmospheric flux predictions. Figure 5 shows the L/E distribution of events from the SuperKamiokande experiment and fits to various scenarios including oscillations, neutrino decay, and neutrino decoherence Ashie et al. [2004]. Neutrino oscillations clearly provide the best description of the atmospheric data.

2. Long Baseline Experiments and Beams

The basic idea behind a long baseline neutrino measurement is simple. A neutrino beam is produced with an energy spectrum which spans the region of interest. This beam is sent through two detectors. The first is located near the neutrino source and measures interactions of the neutrinos before oscillations have occurred, and the second, located a distance L away, detects the neutrinos after oscillations. The baseline L and neutrino energy spectrum (E) are optimized for a particular Δm^2. These experiments can be of two types: disappearance experiments, in which an energy-dependent deficit of neutrinos of the original flavor is measured, or appearance experiments, in which the presence of a new neutrino flavor in the

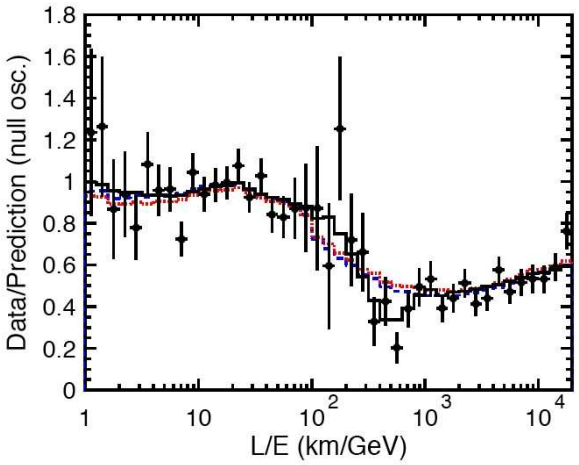

Figure 5: Ratio of the data L/E distribution to the Monte Carlo expectation for atmospheric neutrino events in the SuperKamiokande experiment. The best fit to a neutrino oscillation hypothesis is shown by a solid line, together with neutrino decay (dashed line), and neutrino decoherence (dotted line). Figure taken from Reference Ashie et al. [2004].

beam is observed at the far detector.

In a practical sense these near detectors are of great importance due to the large uncertainties that exist in the neutrino flux calculations and neutrino interactions mechanisms. The underlying difficulty in predicting neutrino fluxes stems from underlying uncertainties in hadron production from thick targets, and uncertainties in neutrino interaction physics are due to the fact that at energies of a few-GeV, many different interaction mechanisms are important and nuclear effects play a large role. Neutrino interactions are tuned to data from previous experiments, typically bubble chamber experiments from the 60's and 70's which had limited statistics and which made very few studies of nuclear effects.

Depending on the specific parameters being measured, appearance / disappearance or wide-band / narrow-band beams can have different strengths and weaknesses, which we will discuss in the specifics in the following sections.

3. K2K

The first long-baseline experiment was the KEK-to-Kamioka (K2K) experiment which collected data from 1999-2004. The neutrino beam was produced from the 12 GeV proton synchrotron at KEK and was sent 250 km to the SuperKamiokande detector. A 1-kton water Cerenkov near detector measured an event sample for comparison in the far detector. Other near detectors were used to make more detailed observations of the neutrino-nucleus interactions and include a scintillating fiber/water target tracker (the SciFi detector), a fine grained scintillator tracking detector (SciBar), a muon range detector, and a lead-glass calorimeter which ran during the first data taking period of the experiment. A total of 1.049×10^{20} POT were delivered to the target of which 0.922×10^{20} were used for physics analyses. Pion and muon monitoring devices provide additional information about the beam. More information about the experiment can be found in Reference Ahn et al. [2006].

A large fraction of neutrino interactions at K2K energies of around 1 GeV are quasi-elastic. These events are identified in the water cerenkov detectors as single-ring events and the neutrino energy is reconstructed using the muon energy and angle with respect to the beam direction and the assumption of quasi-elastic kinematics.

The data in the Near Detectors is used to tune the beam and neutrino interaction Monte Carlos. Once this is done an extrapolation of the measured spectrum in the 1 kton near detector is performed to the far detector and compared with the data. This flux extrapolation is done using the predicted far/near flux ratio from the tuned Monte Carlo and the measured near detector flux spectrum. This spectral comparison together with the oscillation best fit $(\Delta m^2, \sin^2 2\theta) = (2.8 \times 10^{-3}\ \mathrm{eV}^2, 1.0)$ is shown in Figure 6. The confidence interval on the oscillation parameters compared with those from the SuperKamiokande experiment are shown in Figure 7. Both Figures are from Reference Ahn et al. [2006].

The experiment has also performed a ν_e appearance search. They observed one ν_e candidate in the far detector, with an expected background of 1.7 events. At the best fit value from their ν_μ disappearance analysis $\sin^2(2\theta_{13}) > 0.26$ is excluded at the 90% CL Yamamoto et al. [2006].

4. MINOS

The MINOS experiment was designed to make precision measurements of oscillation phenomena at the Δm^2 value probed by atmospheric neutrino experiments. It uses an intense neutrino beam from the NuMI facility and two detectors, a 'Near Detector' located at Fermilab and a 'Far Detector', located 735 km away in the Soudan mine. The goals of the experiment are to make precision measurements of Δm^2_{23}, $\sin^2(2\theta_{23})$, search for sub-dominant $\nu_\mu \rightarrow \nu_e$ oscillations, are search for other exotic phenomena which might manifest themselves in changes in the neutral current events or differences in neutrino and anti-neutrino oscillations. The magnetized far detector is also collecting atmospheric data. Oscillations of neutrinos and anti-neutrinos can be studied separately in this dataset.

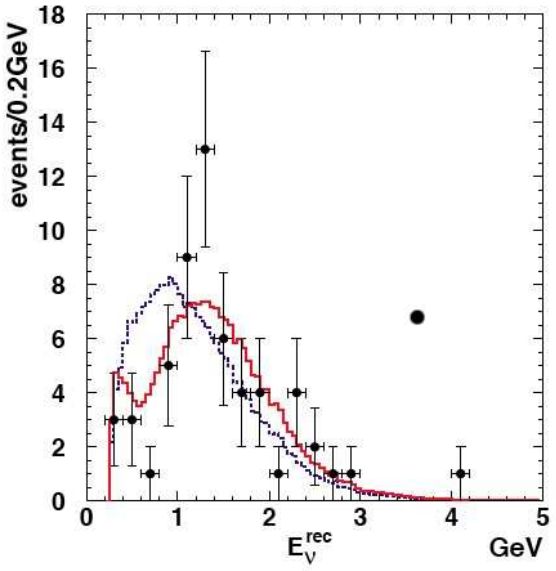

Figure 6: Energy spectrum of single ring events in SuperK for the K2K experiment. Solid line is the best fit spectrum with oscillations and the dashed line is the best fit line without oscillations. Both histograms are normalized to the number of events observed. Figure taken from Reference Ahn et al. [2006].

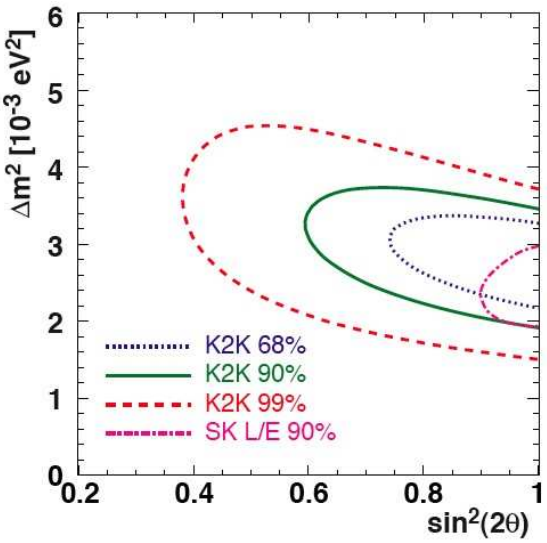

Figure 7: Confidence intervals for the K2K experiment compared with those from the SuperKamiokande L/E analysis Ashie et al. [2004]. Figure taken from Reference Ahn et al. [2006].

In this section I present results from the MINOS experiment for the first 1.27×10^{20} POT. This data was recorded between May 2005 and February 2006. During this period the livetime of the Far Detector was 99.0%. Figure 8 shows a front view of the MINOS Far Detector in the Soudan mine.

4.1. The NuMI Beam

The Fermilab NuMI beam starts with protons from the 120 GeV Main Injector which are extracted in 10μsec spills and bent downward by 58 mrad to point to the Far Detector. This beam is steered onto a 95.4 cm graphite target, and the pions and kaons produced are focused using two parabolic horns spaced 10 m apart. The focused secondaries then travel down a 675 m long evacuated decay pipe where they decay. The target position relative to the first horn can be changed. Doing so modifies the energies of the focused pions and hence the neutrino beam. Most of the data in the first year's running was taken with the target inserted in the first horn 50.4 cm in order to maximize neutrino production in the 1-3 GeV range. Around 1.5×10^{18} POT were taken with the target moved back by 90 cm and 240 cm from this nominal position. The predicted energy spectrum from these three beam configurations is shown in Figure 9. Data in the higher energy configurations was used for systematics studies.

4.2. The MINOS Detectors

The two MINOS detectors are designed to be functionally equivalent. Each is made from alternating planes of 2.54 cm-thick magnetized steel planes and plastic scintillator. The mean field in each detector is 1.3T. The active planes are made from modules of 4.1 cm wide by 1 cm thick co-extruded plastic scintillator strips. Scintillation light emitted in the scintillator is captured in a wavelength-shifting fiber glued into a groove in the strip and transported to multi-anode photodetectors. The Far Detector has 484 8 meter octagonal planes and a mass of 5.4 ktons. The Far Detector photodetectors are 16 pixel and are optically summed with eight fibers incident on each pixel. The Near Detector is composed of several functionally distinct regions with interactions in the target region being comparable to those in the Far Detector. The detector is read out by fast electronics in order to distinguish interactions from individual RF buckets within each Main Injector spill.

All Near Detector data taken within a spill are read out, as are all Far Detector data which satisify minimal energy deposition thresholds within 100 μs of the expected arrival time of the beam.

4.3. Calibration

The calibration of the detector is carried out with stopping and throughgoing cosmic rays, an in-situ light injection system, and test beam data recorded in a small test detector located at CERN. After calibration, the relative energy scales of the two detectors are known to 2%. The single particle energy response for

Figure 8: The MINOS Far Detector.

pions, protons, muons, and electrons was determined in a series of calibration runs using a small, unmagnetized version of the detector. Stopping muons in each of the three detectors are used to relate the calibrations of the separate detectors.

4.4. Analysis

The analysis presented here was carried out as a blind analysis. An energy-dependent fraction of the data from the far detector was hidden from the analyzers. All data in the Near Detector was available for analysis. Once the analysis was defined, and it was decided that a suitable level of agreement between data and Monte Carlo (MC) in the Near Detector had been obtained, the hidden data was released and the final analysis was performed.

The Monte Carlo for this analysis uses GCALOR Zeitnitz and Gabriel [1994] for hadronic shower simulations and NEUGEN3 Gallagher [2002] for the simulation of neutrino interactions. The reconstruction first defines the hits which are part of the event, finds muon tracks in the event, and reconstructs showers. The muon energy resolution varies from 6% at low energy where muons range out in the detector to 13% at high energy where they exit and the energy is determined from curvature. The hadronic shower resolution is approximately $56\%/\sqrt{E}$. The neutrino energy is taken to be the sum of the track and shower energies.

In order to constrain the flux models, data were taken at a series of six runs where the position of the target and the horn magnetic field were varied. Spectra in these configurations were fit to a 15 parameter model which included a parametrization of the hadron production off the target, beam focusing, NC background, ν_μ energy scale and energy offset. The tuned flux MC beam spectrum compared with the nominal MC and data are shown in Figure 9.

Charged current events are selected using a particle ID algorithm which incorporates three pieces of information: the length of the track in the event, the fraction of the event pulse height on the track, and the average pulse height per plane on the track. Figure 10 shows the CC-like PID for data and Monte Carlo in the Near and Far detectors. The contribution from NC events is also shown. The data, particularly in the CC-like region, are well described by the tuned Monte Carlo. CC-like events are selected based on a cut in this variable of -0.1 for ND events and -0.2 for FD events.

Several different approaches to the beam extrapolation were studied. For this first result the *Beam Matrix* method was used. This approach utilizes the fact that neutrinos in both detectors come from the same parent hadrons to relate an energy spectrum in one detector to an energy spectrum in the other. This is done by determining with Monte Carlo a *Beam Matrix* whose elements give the relative probability that the parent hadrons which produce interactions with neutrino energy E_i in the Near Detector will produce

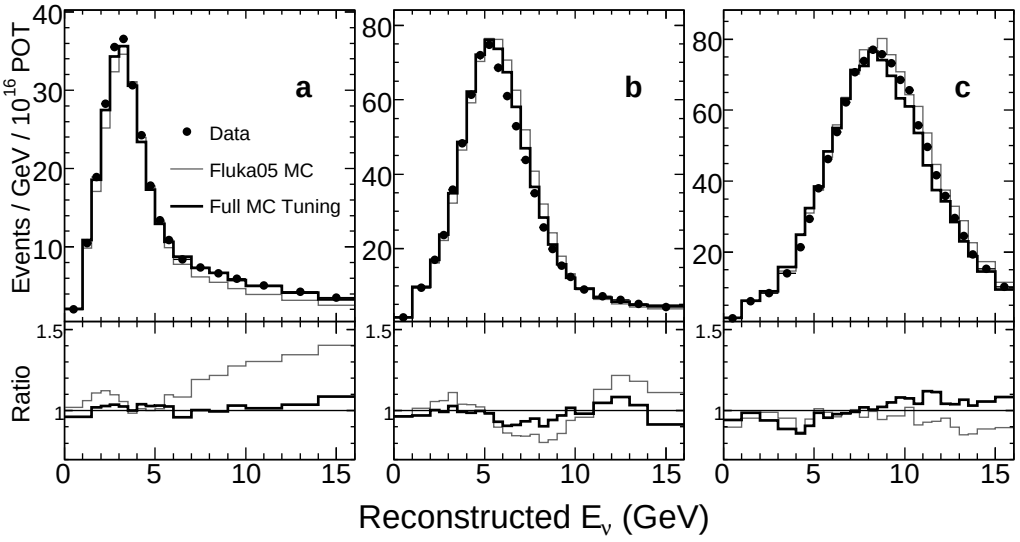

Figure 9: Energy spectra in the MINOS Near Detector for three different beam configurations. Spectra before and after the beam tuning are shown in each case. The lower set of plots shows the ratio of data to MC before and after the tuning. From Reference Michael et al. [2006].

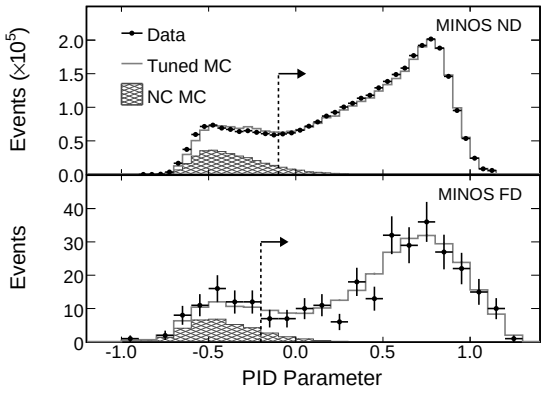

Figure 10: Data and MC predictions for the CC-like PID variable. The Near Detector is shown at the top, Far Detector the bottom. Contributions from NC events are shown by the hatched histogram. From Reference Michael et al. [2006].

neutrinos of energy E_j in the Far Detector. The measured distribution in the Near Detector is first translated into a flux by correcting for acceptance and dividing by the cross section. The beam matrix is then applied to get the far detector flux and the cross section and Far Detector acceptance are applied to obtain the predicted FD spectrum. Another, complementary method called the *ND Fit* method was also studied. This approach attempted to remove any ND data-MC differences remaining after the beam reweighting by adjusting model parameters associated with the neutrino interaction model and detector response. These adjusted parameters are then used to reweight MC predictions for the FD accordingly. The two approaches yield very similar predictions for the FD energy spectrum as can be seen in Figure 11.

The numbers of events observed in the FD compared with MC predictions using the two different extrapolation methods are shown in Table I. The energy spectra is fit to a two generation oscillation probability expression. The fit includes systematic errors due to the the following uncertainties as nuisance parameters: fiducial mass, the absolute hadronic energy scale due to calibration accuracy and intranuclear rescattering effects, NC contamination, muon energy scale, CC cross-sections, relative ND/FD energy calibration, beam extrapolation uncertainties, and reconstruction. For the current level of statistics only the first three sources were non-negligible.

Figure 12 shows the 68 and 90% confidence intervals obtained in this fitting procedure. Also shown are the results from the K2K and SuperK experiments. At 90% CL $(2.31 < |\Delta m^2_{32}| < 3.43) \times 10^{-3}$ eV^2/c^4 and $\sin^2(2\theta_{23}) > 0.78$.

5. OPERA

The OPERA experiment, located in the Gran Sasso laboratory, is performing a ν_τ appearance measurement in the CERN CNGS neutrino beam. The baseline is 730 km. Tau neutrinos are identified in the detector through the nuclear emulsion technique utilized for the ν_τ discovery by the DONUT experiment Kodama et al. [2001]. The analysis focuses on 1-prong ν_τ decay modes which comprise 85% of the decays. The mean neutrino energy is 17 GeV and the detector is expected to record around 6200 ν_μ interactions and

Table I Numbers of events observed and expected in the MINOS Far Detector.

Data Sample	Data	Expected Matrix Method Unoscillated	Data/MC Matrix Method	Expected Fit Method Unoscillated
$\nu_\mu < 30$ GeV	215	336 ± 21	0.64 ± 0.08	332.8
$\nu_\mu < 10$ GeV	122	239 ± 17	0.51 ± 0.08	237.7
$\nu_\mu < 5$ GeV	67	168 ± 12	0.45 ± 0.09	168.6

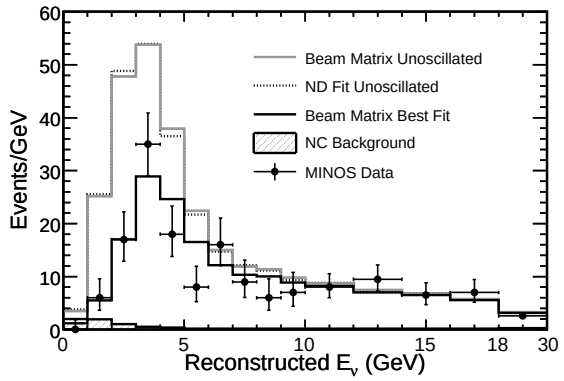

Figure 11: The MINOS Far Detector spectrum compared to the predictions for no oscillations and with a best fit oscillation model. The unoscillated prediction from two beam extrapolation methods are shown. From Reference Michael et al. [2006].

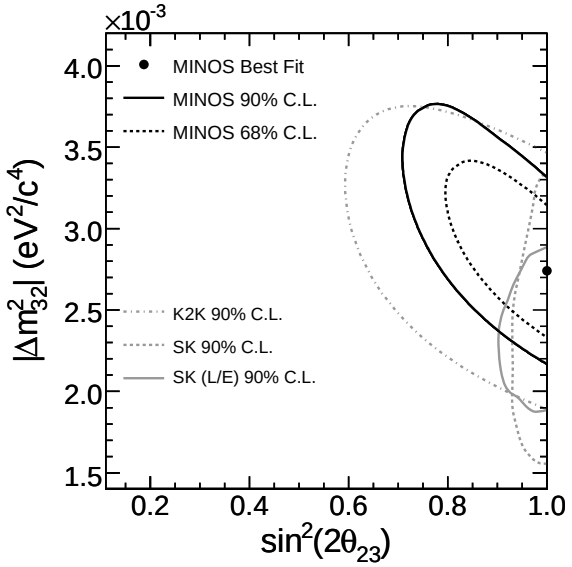

Figure 12: Confidence intervals from MINOS data including systematic errors. Also shown are the contours from the previous highest precision experiments Ashie et al. [2004, 2005], Aliu et al. [2005]. From Reference Michael et al. [2006].

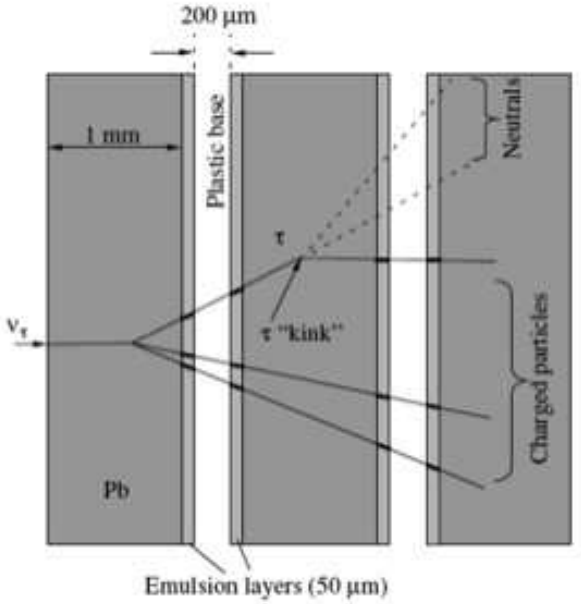

Figure 13: The basic topology for tau identification in the OPERA emulsion bricks.

27 ν_τ interactions per year for a Δm^2_{23} of 2.4×10^{-3} eV^2 Di Capua [2006].

The basic element of the detector is a brick of $10.2 \times 12.7 \times 7.5\,\mathrm{cm}^3$ made up of alternating 1 mm thick lead plates and emulsion films. Each emulsion sheet consists of a plastic base with two emulsion layers of around 50 μm on each side. The entire detector is built up from around 200,000 bricks in total. Walls of these bricks are interspersed with electronic detectors which provide tracking and identify the brick in which the interaction occurred. These Target Tracker (TT) planes consist of orthogonal arrangements of scintillator strips. The full detector is made up of two sections each containing 31 brick planes and TT planes. Following each section is a muon spectrometer composed of a dipole magnetic field, RPC chambers and drift tubes for precision tracking. Figure 13 shows the topology of the tau decay candidate in the emulsion layers. The target mass of the detector is 1.8 ktons. A picture of the detector taken in June 2006 is shown in Figure 14.

Bricks identified by the electronic detectors as con-

taining interactions are moved robotically in real-time and exposed to cosmic rays at the surface to produce alignment tracks. The bricks are sent to automated scanning stations (one in Japan, the other in Europe) where the developed film is scanned and tau decay candidates are identified.

The CNGS beam was commissioned in July-August 2006 and ran until the end of 2006. Neutrino interactions were observed in the OPERA electronic detectors and exhibited the expected timing and angular distributions. The experiment is ready for analysis of emulsion data in 2007.

Backgrounds to the tau decay search come from the decays of charm hadrons, hadron reinteractions and large angle muon scattering. The sensitivity of the experiment depends strongly on the true value of Δm^2_{23}. The results from the MINOS experiment, which indicate that Δm^2_{23} is in the upper region suggested by the Super-K results, bode well for the experiment. In five years of data taking with 4.5×10^{19} POT/year the experiment has an expected signal of 19.9 events if $\Delta m^2_{23} = 3.0 \times 10^{-3}$ eV^2 and an expected signal of 12.8 events if $\Delta m^2_{23} = 2.4 \times 10^{-3}$ eV^2, with an expected background of 1.0 events Di Capua [2006]. (These numbers assume full mixing). The number of expected background events may be reduced by around 20% if improvements in the identification and measurement of muon tracks in the bricks come to fruition. The overall efficiency for tau detection is 9.1% Gustavino [2006].

The experiment can also carry out a ν_e appearance measurement in the detector and in five years nominal running can improve the 90% CL limit on θ_{13} to 7.1° Gustavino [2006].

6. Next Goals

The goals for the next generation of experiments are to measure the two remaining parameters in the PMNS matrix - θ_{13} and δ_{CP} - and determine the mass hierarchy. In determining θ_{13} one is looking for oscillation effects at the atmospheric Δm^2. Accelerator experiments like T2K and NOνA will be attempting to do so via $\nu_\mu \rightarrow \nu_e$ appearance, and reactor experiments will attempt to do so with ν_e disappearance measurements over long baselines.

Generally speaking the challenge for long-baseline neutrino experiments is identifying a small ν_e appearance signal in the presence of backgrounds coming from neutral current interactions and intrinsic electron neutrinos in the beam. The experiments require large detectors with excellent pattern recognition capabilities, in particular for electron / π° separation. For a particular baseline the peak oscillation energy is fairly well defined and an ideal beam would be a narrow band beam at this energy, which would maximize the oscillation signal while reducing NC feeddown from higher energy neutrinos.

The necessary beams can be produced by placing the detectors off-axis. At an off-axis location the neutrino energy spectrum is closer to a narrow band beam due to decay kinematics. This fact will be exploited by both the T2K and NOνA experiments to tune their beam energies and reduce NC backgrounds.

A key aspect of future developments is the need for complementarity in order to fully disentangle the mixing parameters and mass hierarchy. Matter effects coming from ν_e coherent scattering from electrons in the earth change the effective mass of the electron neutrino states and produce a splitting between the neutrino and anti-neutrino oscillation probabilities. These effects become larger at longer baselines and higher energies. This asymmetry exists even in the absence of CP violations.

6.1. T2K

The Tokai to Kamioka (T2K) experiment will utilize a new neutrino beamline at J-PARC to send an intense, 2.5° off-axis beam to the refurbished Super-Kamiokande (Super-K III) detector located 295 km away. The beamline is currently under construction and will consist of a 750 kW conventional neutrino beam produced from the 50 GeV J-PARC proton beam. The beamline is expected to be completed in 2009. The mean neutrino energy of the beam of 600 MeV is optimized for the appearance signature at this baseline. The experiment will yield a dramatic improvement over the statistics of the K2K experiment, with a design intensity of 1×10^{21} POT/year compared with the 1×10^{20} POT obtained in the six years of K2K operations.

At these low energies neutrinos interact mainly quasi-elastically, in which the outgoing muon produces a single Cerenkov ring. The determination of the muon angle and energy can be used to reconstruct the neutrino energy under the assumption of quasi-elastic kinematics even though the outgoing proton is not observed. A neutrino energy resolution of around 10% can be obtained using this technique. The experiment will utilize three near detectors, one on-axis at 280 m to measure the beam profile, a two off-axis at 280 m and 22 km to measure the unoscillated flux to Super-K and determine cross sections.

In 5 years of running the experiment will have 103 signal events with a beam ν_e background of 13 events and other backgrounds of 10 events Nakadaira [2006]. This assumes $\Delta m^2_{23} = 2.5 \times 10^{-3}$ eV^2, $\delta_{CP} = 0$, $\sin^2(2\theta_{13}) = 0.1$, and $\sin^2(2\theta_{23}) = 1.0$. For this set of parameters the 90% CL sensitivity (including systematics) is $\sin^2(2\theta_{13}) = 0.008$ Nakadaira [2006].

If this program, known as T2K-I, is successful in making a measurement of θ_{13}, it opens the door to

Figure 14: The OPERA detector.

a search for CP violation in the neutrino sector. An upgrade path, T2K-II, is also being investigated which require a J-PARC upgrade from 750 kW to 4 MW.

6.2. NOνA

The NuMI Off-Axis ν_e Appearance (NOνA) experiment utilizes an off-axis beam, improvements to the NuMI facility, and a 20-25 kton detector located 810 km away to perform a precise ν_e appearance experiment using both neutrinos and antineutrinos. Because of the longer baseline and importance of matter effects, comparing neutrino and antineutrino oscillations from this experiment gives additional handles on measuring the mass hierarchy.

Crucial to the success of the experiment are a series of proposed upgrades to NuMI and the accelerator complex. These would occur over three phases and would increase the intensity from its current value of around 250 kW to 430 kW (2009), 700 kW (2012), and 1.2 MW (2013). The second two phases would take place after the Tevatron is shut down Kopp [2006]. The 3σ discovery potential for the experiment after an exposure of 60×10^{20} POT is shown in Figure 15 Feldman [2006].

The detector would be located in a surface site in Ash River, MN and would consist of extruded 15.7 m long PVC cells filled with liquid scintillator being read out by looped WLS fibers in the cell carrying light to APDs. The transverse dimensions of the cells are 6 cm by 3.9 cm and provide a detector that is nearly

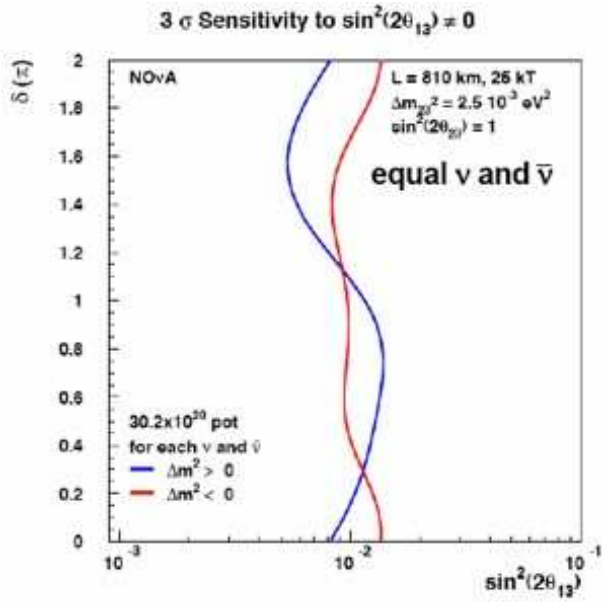

Figure 15: The 3 σ discovery potential of the NOνA experiment. This limit assumes equal neutrino and anti-neutrino running.

completely active.

7. Conclusion

There is a global effort underway to explore with increasing precision the PMNS matrix which may hold the key to understanding the matter-antimatter asymmetry in the universe. The groundbreaking discoveries that opened the door to this field came from a number of ingenious experiments using neutrinos from a variety of sources including the sun, atmosphere, and nuclear reactors. A current generation of experiments including MINOS, OPERA, and miniBoone is underway to use accelerator-produced neutrino beams to measure the mixing parameters with more detail and resolve the questions surrounding the LSND result. The remaining questions - measuring θ_{13}, δ_{CP}, and determining the mass hierarchy - may be addressed within the next decade by T2K-I and NOνA or may not be fully resolved until the following generation of experiments. In any case long-baseline experiments will play an important role in this experimental area for the forseeable future.

Acknowledgments

The author would like to thank for the organizers of the PIC 2006 conference for their efforts in producing an interesting meeting and a stimulating environment for discussion. This work is supported by Department of Energy grant DE-FG02-92ER40702.

References

Z. Maki, M. Nakagawa, and S. Sakata, Prog. Theor. Phys. **28**, 870 (1962).
B. Pontecorvo, Sov. Phys. JETP **26**, 984 (1968).
G. L. Fogli et al. (2006a), hep-ph/0608060.
G. L. Fogli, E. Lisi, A. Marrone, A. Palazzo, and A. M. Rotunno, Prog. Part. Nucl. Phys. **57**, 71 (2006b).
S. Eidelman et al. (Particle Data Group), Phys. Lett. **B592**, 1 (2004).
J. N. Bahcall, A. M. Serenelli, and S. Basu, Astrophys. J. **621**, L85 (2005), astro-ph/0412440.
B. T. Cleveland et al., Astrophys. J. **496**, 505 (1998).
M. Altmann et al. (GNO), Phys. Lett. **B616**, 174 (2005), hep-ex/0504037.
W. Hampel et al. (GALLEX), Phys. Lett. **B447**, 127 (1999).
J. N. Abdurashitov et al. (SAGE), J. Exp. Theor. Phys. **95**, 181 (2002), astro-ph/0204245.
Y. Fukuda et al. (Kamiokande), Phys. Rev. Lett. **77**, 1683 (1996).
J. Hosaka et al. (Super-Kamkiokande), Phys. Rev. **D73**, 112001 (2006), hep-ex/0508053.
B. Aharmim et al. (SNO), Phys. Rev. **C72**, 055502 (2005), nucl-ex/0502021.
K. Eguchi et al. (KamLAND), Phys. Rev. Lett. **90**, 021802 (2003), hep-ex/0212021.
T. Araki et al. (KamLAND), Phys. Rev. Lett. **94**, 081801 (2005), hep-ex/0406035.
Y. Ashie et al. (Super-Kamiokande), Phys. Rev. Lett. **93**, 101801 (2004), hep-ex/0404034.
M. H. Ahn et al. (K2K), Phys. Rev. **D74**, 072003 (2006), hep-ex/0606032.
S. Yamamoto et al. (K2K), Phys. Rev. Lett. **96**, 181801 (2006), hep-ex/0603004.
C. Zeitnitz and T. A. Gabriel, Nucl. Instrum. Meth. **A349**, 106 (1994).
H. Gallagher, Nucl. Phys. Proc. Suppl. **112**, 188 (2002).
D. G. Michael et al. (MINOS), Phys. Rev. Lett. **97**, 191801 (2006), hep-ex/0607088.
Y. Ashie et al. (Super-Kamiokande), Phys. Rev. **D71**, 112005 (2005), hep-ex/0501064.
E. Aliu et al. (K2K), Phys. Rev. Lett. **94**, 081802 (2005), hep-ex/0411038.
K. Kodama et al. (DONUT), Phys. Lett. **B504**, 218 (2001), hep-ex/0012035.
F. Di Capua (OPERA), PoS **HEP2005**, 177 (2006).
C. Gustavino (OPERA), J. Phys. Conf. Ser. **39**, 326 (2006).
T. Nakadaira, Talk at Neutrino 2006 http://neutrinosantafe06.com/downloads/Session7/7.9Nakadaira.pdf, (2006).
S. E. Kopp (2006), hep-ex/0612025.
G. Feldman (2006), http://www.fnal.gov/directorate/program_planning/P5/P5_Apr2006/Talks/Feldman.pdf.